

Robust Elastic Structure Preserving Control for High Impedance Rendering of Series Elastic Actuator

Hyunwook Lee¹, Jinoh Lee², Manuel Keppler², and Sehoon Oh³

Abstract—In this paper, a new robust approach is proposed to address the limitation of impedance rendering for Series Elastic Actuators (SEA). The concept of Elastic Structure Preserving (ESP) control allows for the attachment of desired load-side dynamics to the SEA while maintaining a passivity condition, regardless of the parameters for the attached dynamics. The characteristics of ESP control are revisited and translated in the frequency domain, which grants a new perspective to identify its advantages compared to conventional impedance control in terms of passivity. Additionally, we analyze the degradation of performance due to unwanted disturbance and uncertainties in spring stiffness and motor inertia, and a new form of the robust ESP method is proposed by endowing disturbance rejection capability and robustness against uncertainty.

Index Terms—Compliance and Impedance Control, Flexible Robotics, Robust Control

I. INTRODUCTION

RECENTLY, there has been a growing demand for collaborative robots in various fields of application. To ensure safe and reliable interactions between robots and humans, safety and reliability have become crucial considerations. One solution to these requirements is the use of series elastic actuators (SEAs). These actuators have been developed to enable compliant behaviors for safer operation [1]. SEAs have the capability of measuring force without a force sensor and reducing shock through their intrinsic elasticity. Due to these advantageous properties, SEAs have been successfully employed in high-performance force control where safety and compliance are of paramount importance [2], [3].

Impedance control is widely employed for SEAs to take advantage of their high fidelity from the inherent force control capability. Impedance-controlled SEAs have been deployed in diverse robot platforms such as humanoids and exoskeletons

[4]–[8] providing compliant interactions. On the other hand, for performing practical tasks, high impedance is essential for rejecting disturbances or interacting with heavy objects [9]. However, SEAs are well suited for interaction with a low impedance while implementing high impedance functions can be challenging [10]–[13].

In control of interaction tasks, priority should be given to stability over performance. In addition to the classical stability for free movement scenarios, systems that engage in frequent interactions must take into account the environment. Coupled stability refers to the stability of a controlled system coupled to its environment. The violation of the system’s passivity may fail to guarantee this coupled stability when interacting with a stiff environment [14]. For this stability, the passivity concept has been widely studied [14]–[16].

Nevertheless, the passivity-based analysis impedes the performance of impedance-controlled SEA because passivity can be violated when the impedance is increased beyond the spring stiffness through conventional cascade impedance control (CIC) [10]–[13]. In [10], [11], a limitation in stiffness was revealed when using only a pure stiffness in impedance control. Furthermore, this limitation was recognized even with the adoption of the viscoelastic impedance model [12] and the use of various impedance structure: collocated motor feedback, impedance with additional inner velocity feedback, and admittance control [13]. To address this issue, time-domain approaches have been developed to observe passivity in real-time and to relax passivity violations by real-time stiffness modification [17]. However, this approach does not inherently allow for high stiffness rendering as it reduces the desired stiffness when passivity is violated.

To overcome the limit of the achievable stiffness, the concept of Elastic Structure Preserving (ESP) control has been developed [18]. It enables the direct interconnection of desired dynamics to the load-side. Particularly, allowing for the interconnection of impedance elements. Crucially, with these impedance elements, the passivity of the closed loop is guaranteed, regardless of the parameters associated with the attached dynamics [18]–[20]. This desirable property is directly inherited from the structure-preserving nature of the ESP approach, as the generated closed-loop dynamics is solely constituted by passive elements, namely masses, springs, and dampers. This characteristic intuitively suggests the parameter-independent passivity of the closed loop. However, this approach, dependent on the dynamic model of SEA, is inherently vulnerable to model uncertainties. Furthermore, the controlled

Manuscript received: September 17, 2023; Revised December 18, 2023; Accepted January 29, 2024. This paper was recommended for publication by Editor Jaydev P. Desai upon evaluation of the Associate Editor and Reviewers’ comments. This work was fully funded by NAU Robotics Co., Ltd. (Corresponding author: Sehoon Oh.)

¹Hyunwook Lee is with the Department of Mechatronics Engineering, Gyeongsang National University, Jinju, Republic of Korea. (e-mail: koma0711@gmail.com)

²Jinoh Lee and Manuel Keppler are with the Institute of Robotics and Mechatronics, German Aerospace Center (DLR), 82234 Wessling, Germany. Jinoh Lee is also an adjunct professor at the Department of Mechanical Engineering, Korea Advanced Institute of Science and Technology (KAIST), Yuseong-gu, 34141 Daejeon, Republic of Korea. (e-mail: jinoh.lee@dlr.de; manuel.keppler@dlr.de)

³Sehoon Oh is with the Department of Robotics Engineering, DGIST, Daegu, Republic of Korea. (e-mail: sehoon@dgist.ac.kr)

Digital Object Identifier (DOI): see top of this page.

©2024 IEEE. Personal use of this material is permitted. Permission from IEEE must be obtained for all other uses, in any current or future media, including reprinting/republishing this material for advertising or promotional purposes, creating new collective works, for resale or redistribution to servers or lists, or reuse of any copyrighted component of this work in other works. DOI: 10.1109/LRA.2024.3366016

system's performance deteriorates in the face of disturbance¹, as it lacks a separate function for disturbance rejection. This study investigates the impact of these factors on the performance of ESP control and proposes a robust controller to overcome these limitations.

The contributions of the paper can be listed as follows.

- 1) By analyzing ESP control in the frequency domain, we offer a new perspective and identify several advantages over CIC control methodologies.
- 2) Through the addition of a disturbance observer, we present a robust ESP (R-ESP) control design. It can render any desired stiffness while ensuring closed-loop stability and passivity in the presence of uncertain spring stiffness and motors inertia parameters.
- 3) An extended stability analysis includes the impact of filters. Comparing R-ESP and ESP designs, it demonstrates that R-ESP exhibits a higher phase margin in the presence of filters, indicating superior robustness.

II. ELASTIC STRUCTURE PRESERVING CONTROL TO OVERCOME STIFFNESS LIMITATION OF SEA

An intrinsic spring component in SEAs allows for precise force measurement and control [3]. This enables SEAs to be well-suited for applications involving interaction with a variety of environments. However, CIC guarantees limited range of active spring rendering based on passivity analysis. In this section, we analyze this limitation and introduce ESP control as a solution to overcome this limitation.

Initially, the dynamics are derived and subsequently investigated to identify the drawbacks associated with conventional impedance control. Our investigations employ frequency domain analysis, which is based on the dynamics previously derived. Furthermore, the frequency domain analysis of the ESP control effectively confirms its advantages.

A. Conventional understanding of Stiffness Limit of SEAs

Figure 1(a) shows a schematic diagram of the SEA that consists of a motor, a spring, and a load. The motor is rotated by the motor torque τ_m which consists of the motor inertia J_m and the motor viscous friction B_m , and its angular position is given as θ . The load is composed of its inertia M_l and damping B_l , and its position is given as q . The spring K , which has the torsional spring stiffness of 2.208 Nm/rad, generates the spring torque $\tau_s = K(N^{-1}\theta - q)$ and transmit the torque to the load and the motor. N is gear ratio. τ_e indicates external torque.

The SEA dynamics can be expressed in the time domain as follows:

$$M_l \dot{q} + B_l \dot{q} = \tau_s + \tau_e \quad (1)$$

$$J_m \ddot{\theta} + B_m \dot{\theta} + N^{-1} \tau_s = \tau_m + d \quad (2)$$

where d is a disturbance acting on the motor dynamics.

The dynamics of SEA can be represented in the Laplace domain, enabling an intuitive understanding of controllers'

¹The disturbance in this study is defined as an unwanted motor-side disturbance that needs to be eliminated. This is distinct from an external force that creates compliant interactions with impedance control.

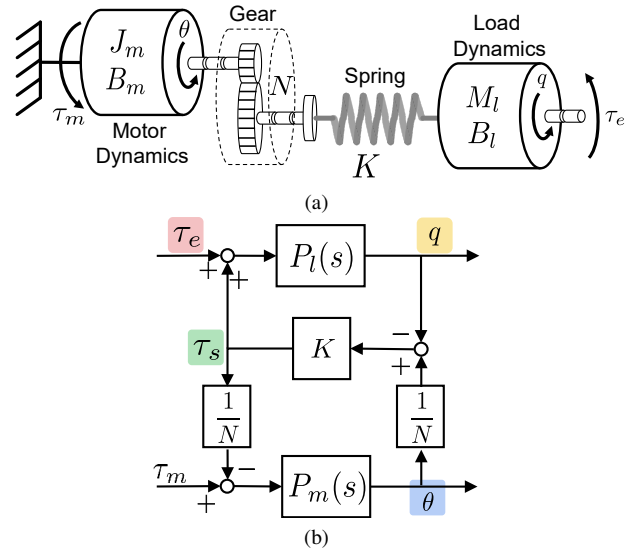


Fig. 1. (a) A schematic diagram of the SEA, and (b) its block diagram.

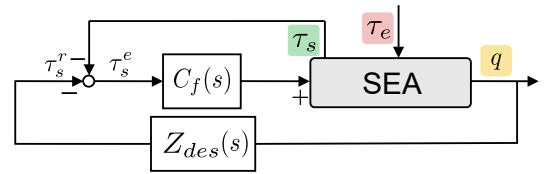


Fig. 2. Block diagram of SEA system with cascade impedance control. The impedance controller Z_{des} and inner force controller C_f are applied. τ_s^r and τ_s^e indicate reference and error of spring force.

effectiveness by analyzing their frequency responses. This is expressed using a block diagram as illustrated in Fig. 1(b). The motor dynamics $P_m(s)$ and the load dynamics $P_l(s)$ are given in the Laplace domain as follows:

$$P_m(s) = \frac{1}{J_m s^2 + B_m s}, P_l(s) = \frac{1}{M_l s^2 + B_l s} \quad (3)$$

The passivity of linear systems can be analyzed in the frequency domain through the evaluation of the phase characteristics of controlled impedance [10]. It is well known that a phase deviation outside the range of -90° to 90° results in a non-passive system [14]. Therefore, the passivity conditions of closed-loop systems can be compared by analyzing the phase characteristics of the transfer functions,

The impedance control of the SEA is formulated using the obtained SEA dynamics. The control strategy follows the CIC framework, shown in Fig. 2, which comprises a force controller in the inner loop and an impedance controller in the outer loop. The inner force controller, denoted as $C_f = \Lambda_p + \Lambda_d s$, consists of a proportional gain Λ_p and a differential gain Λ_d [21]. The desired impedance Z_{des} is given as follows:

$$Z_{des} = K_q + D_q s, \quad (4)$$

where D_q and K_q are the desired damping and stiffness of impedance, respectively. D_q should be designed properly depending on the application of impedance control, however, this section focuses on the effect of K_q because it is the most critical factor causing the passivity violation.

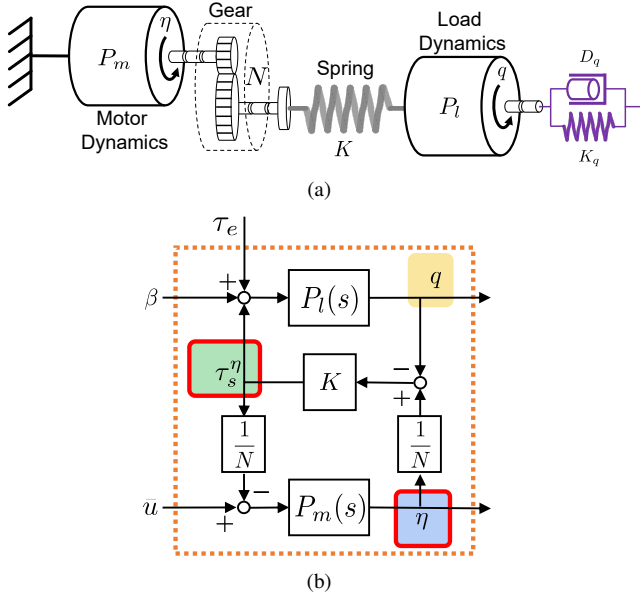


Fig. 3. (a) A schematic diagram of SEA with the ESP and (b) its equivalent block diagram.

By implementing CIC, the controlled impedance from the load velocity to the spring torque can be derived in the Laplace domain.

$$Z^{CIC}(s) = \frac{-\tau_s}{qs} = \frac{N^{-1}KZ_{des}C_f + KP_m^{-1}}{N^{-1}KC_f + N^{-2}K + P_m^{-1}} \frac{1}{s}. \quad (5)$$

The passivity violation is confirmed by checking the positive realness of the derived transfer function [14]. The real part of the above equation is derived, as follows:

$$\begin{aligned} \Re(Z^{CIC}) &= \frac{NB_mK(N^{-1}K - K_q\Lambda_p + K\Lambda_p)}{(NB_m\omega + K\Lambda_d\omega)^2 + (K\Lambda_p + N^{-1}K - NJ_m\omega^2)^2} \\ &+ \frac{N\Lambda_dK(J_mK\omega^2 - J_mK_q\omega^2 + K_qN^{-2}K)}{(NB_m\omega + K\Lambda_d\omega)^2 + (K\Lambda_p + N^{-1}K - NJ_m\omega^2)^2}, \\ &\geq 0, \end{aligned} \quad (6)$$

The passivity condition is not be satisfied when K_q is higher than K regardless of the force gains (Λ_p , Λ_d). This condition is expressed as the following inequality.

$$1 \geq \frac{K_q}{K}. \quad (7)$$

B. Interpretation of ESP in frequency domain

The following subsection provides a detailed explanation of the ESP control and demonstrates, through the Laplace domain analysis, how it guarantees passivity even when high stiffness is rendered.

The concept of the ESP control consists of two steps. Firstly, it involves altering the coordinates to exert a direct influence on the load side using the motor torque. Secondly, it applies supplementary dynamics (damping and stiffness) directly to the load dynamics, as depicted in Fig. 3.

The desired dynamics, denoted as β , can be interpreted as a virtual input acting on the load, as illustrated in Fig. 3.(b)

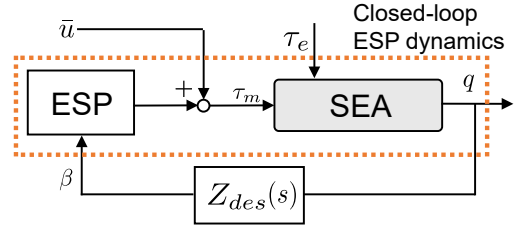


Fig. 4. Block diagrams of impedance-controlled SEA with ESP control.

and shown in [20], [22]. The motor torque τ_m for the ESP control is designed considering the input β as follows:

$$\tau_m = \bar{u} + NK^{-1}(J_m\ddot{\beta} + B_m\dot{\beta} + N^{-2}K\beta), \quad (8)$$

where \bar{u} is additional input that is utilized as the most outer control input. The resulting dynamics is derived as

$$M_l\ddot{q} + B_l\dot{q} - \beta = \tau_s^\eta + \tau_e \quad (9)$$

$$J_m\ddot{\eta} + B_m\dot{\eta} + N^{-1}\tau_s^\eta = \bar{u} + d, \quad (10)$$

where $\eta = \theta - NK^{-1}\beta$ is a new motor angle coordinate. $\tau_s^\eta = K(N^{-1}\eta - q)$ is the spring force in the new coordinate. Notice that the resulting dynamics preserve the elastic structure of SEA even though it is reformulated using the new input β and the new angle η .

The new input β is designed to add desired impedance, as follows:

$$\beta = -K_q(q - q_d) - D_q\dot{q}, \quad (11)$$

where K_q is stiffness and D_q is viscous damping on the load side. Finally, the ESP control renders the desired stiffness and damping directly to the load dynamics as illustrated in Fig. 3(a).

The ESP-controlled system is also expressed in the Laplace domain. The closed-loop equation with the ESP control is derived based on the SEA dynamics and ESP control.

$$Z^{ESP}(s) = \frac{-\tau_s}{qs} = \frac{N^2(K_q + K)P_m^{-1} + KK_q}{N^2P_m^{-1} + K} \frac{1}{s}. \quad (12)$$

The real part of the second term in (12) is determined as follows:

$$\Re(Z^{ESP}) = \frac{B_mN^{-2}K^2}{(B_m\omega)^2 + (N^{-2}K - J_m\omega^2)^2} \geq 0 \quad (13)$$

The above inequality holds at all frequencies. Thus, we can conclude that the ESP-controlled system is always passive regardless of the system's parameters.

C. Comparison of CIC and ESP on stiffness limitation

The derived impedance functions enable a comparison of frequency responses under various desired stiffness conditions. Figure 5(a) shows the frequency responses of the natural impedance of the SEA and of the impedance rendered by using CIC. Parameters are set for simulation : $J_m = 7.08e-5 \text{ kg}\cdot\text{m}^2$, $B_m = 3.12e-4 \text{ Nm}\cdot\text{s}/\text{rad}$, $M_l = 6.96e-5 \text{ kg}\cdot\text{m}^2$, $B_l = 3.12e-4 \text{ Nm}\cdot\text{s}/\text{rad}$, $K = 2.208 \text{ Nm}/\text{rad}$, $N = 1$. Without loss of generality, we set the motor and load inertia to have similar values and set the gear ratio to 1. The closed-loop impedance

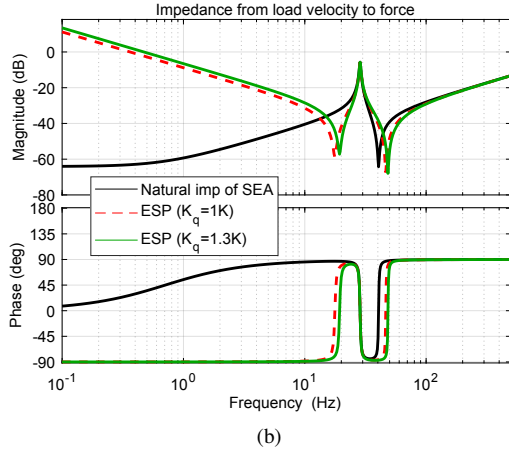
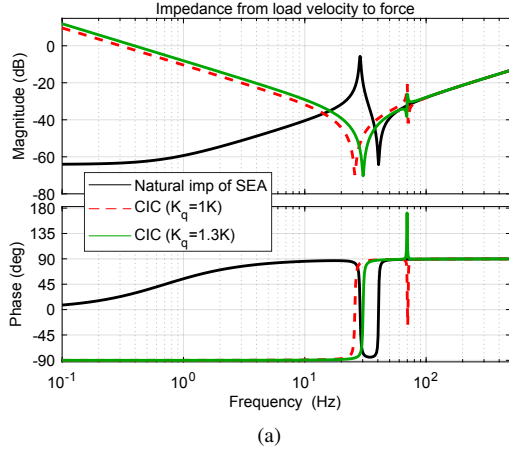


Fig. 5. Impedances of (a) CIC and (b) ESP depending on various desired stiffness (from the load velocity \dot{q} to the external torque τ_e).

with CIC is altered by the desired impedance; specifically, the CIC primarily influences the low-frequency region of the natural impedance of the SEA, adjusting it to match the desired stiffness model (K_q/s).

The phase at frequencies above the resonance varies significantly with changes in the desired stiffness values as in Fig. 5(a). When K_q is set to a value less than K , the phase remains within -90° and the passivity condition is satisfied. Conversely, when K_q is set to a value greater than K , the phase exceeds 90° at high frequencies, indicating a violation of passivity. These results are consistent with the positive realness analysis for passivity violations in Eq. (7).

Figure 5(b) illustrates the results of impedance using the ESP control. The magnitude and phase at frequencies below the resonance are comparable to those achieved using CIC. However, the closed-loop impedance with ESP control maintains a phase range within $\pm 90^\circ$, thus ensuring passivity. This means that the desired stiffness through ESP control is effectively rendered while preserving the structure of the SEA, as in Fig. 3. This structural preserving characteristic is a significant advantage of ESP over CIC, as CIC disrupts the structure of the SEA to render the desired stiffness, leading to potential passivity violations. Therefore, ESP is a safer option than CIC in terms of passivity.

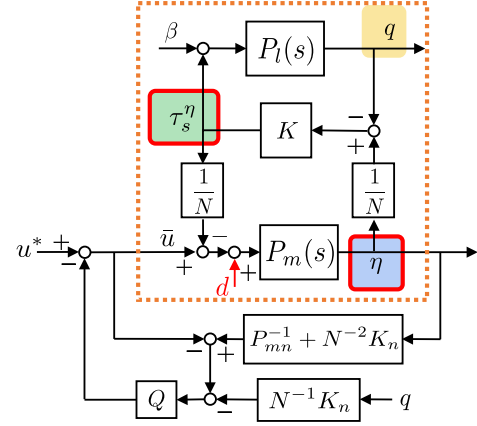


Fig. 6. Block diagram of R-ESP control.

III. ROBUST ELASTIC STRUCTURE PRESERVING CONTROL

The performance of impedance rendering can be degraded by the presence of disturbances and uncertain model parameters, leading to potential passivity violations. To handle these issues, this section introduces a new robust controller that takes advantage of the capabilities of Disturbance Observer (DOB) [3], [23], [24] and ESP.

A. Design of Robust ESP

The robust elastic structure preserving (R-ESP) control, is designed to provide the function of disturbance rejection on top of the ESP control. Figure 6 illustrates the configuration of the R-ESP, where the closed-loop dynamics with the ESP control is placed in the inner loop and wrapped with the DOB. Note that the closed-loop dynamics with the ESP control, colored in orange, correspond to the equivalent structure in which the ESP is applied to the SEA as shown in Fig. 3. The motor position η in the new coordinate system is fed back to the DOB, instead of the original motor position value. The DOB utilized in this paper is a Motor Disturbance Observer (MDOB), which is specifically designed for SEAs to reject disturbances in motor dynamics. The control input of MDOB is derived as follows:

$$u_{mdob} = -\frac{Q(s)}{1-Q(s)} \left[(P_{mn}^{-1}(s) + \frac{K_n}{N^2})\eta - \frac{K_n}{N}q \right], \quad (14)$$

where P_{mn} and K_n are nominal models of motor dynamics and spring, respectively. Finally, the control input for the motor torque to implement the R-ESP control is derived as follows:

$$u^{R-ESP} = \frac{1}{1-Q(s)} u^* + u_{mdob} + u_{esp}. \quad (15)$$

$$u_{esp} = \left(\frac{NP_{mn}^{-1}(s)}{K_n} + \frac{1}{N} \right) \beta, \quad (16)$$

$$u^* = -D_\eta s q, \quad (17)$$

where u_{esp} is the control input for the basic ESP control and u^* is motor damping control.

B. Disturbance rejection with R-ESP

The closed-loop dynamics with R-ESP is represented in the Laplace domain by substituting the control input of R-ESP in (15) into the motor torque.

$$M_l q s^2 + B_l q s = \tau_s^\eta + \tau_e + \beta \quad (18)$$

$$J_m \eta s^2 + B_m \eta s + N^{-1} \tau_s^\eta - d = \frac{1}{1 - Q(s)} u^* + u_{mdob}. \quad (19)$$

And then substituting u_{mdob} in (14), the resulting closed-loop dynamics is derived as follows:

$$J_m \eta s^2 + B_m \eta s + N^{-1} \tau_s^\eta - [1 - Q(s)]d = u^*. \quad (20)$$

The Q filter of R-ESP control only influences the disturbance. Closed-loop transfer function from the disturbance to the load position is derived as follows:

$$\frac{q}{d} = (1 - Q) \frac{NK}{(P_l^{-1} + K_q)(N^2 P_m^{-1} + K) + N^2 K P_m^{-1}}. \quad (21)$$

Assuming $Q(s) = 1$, only the disturbance is rejected while preserving the dynamics.

IV. ROBUSTNESS ANALYSIS OF CONTROLLERS IN THE PRESENCE OF UNCERTAINTY

In this section, the performance degradation of the ESP in the presence of uncertainty is analyzed, and the achievable stiffness of the ESP and R-ESP control is quantitatively evaluated based on the level of uncertainty.

A. Passivity condition of controllers for impedance rendering

The spring plays a crucial role in the SEA, and its uncertainty is a commonly encountered issue. Hence, our initial focus is on examining the uncertainty associated with stiffness.

Using the ESP control, the closed-loop impedance is derived in the Laplace domain as follows:

$$Z_{unct}^{ESP}(s) = \frac{1}{P_l s} + \frac{N^2(K K_q K_n^{-1} + K) P_m^{-1} + K K_q}{N^2 P_m^{-1} + K} \frac{1}{s}. \quad (22)$$

The real part of the equation is derived as follows:

$$\Re(Z_{unct}^{ESP}) = \frac{B_m K N^{-2} (K K_q K_n^{-1} + K - K_q)}{(B_m \omega)^2 + (N^{-2} K - J_m \omega^2)^2}. \quad (23)$$

The closed-loop system is passive when the spring stiffness is greater than the nominal stiffness ($K \geq K_n$). Conversely, when the spring stiffness is less than the nominal stiffness ($K_n \geq K$), the passive condition of the closed-loop system is derived as follows:

$$\frac{K_n/K}{K_n/K - 1} \geq \frac{K_q}{K}. \quad (24)$$

Figure 7 illustrates the achievable stiffness of the ESP and CIC in relation to the uncertainty level. The x-axis represents the uncertainty ratio (K_n/K) in (24), while the y-axis represents the stiffness ratio. The stiffness ratio indicates the proportion of passively achievable stiffness to spring stiffness. That is, the area beneath the plotted line represents all the

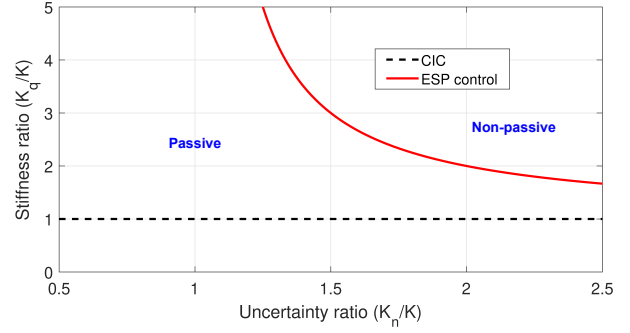


Fig. 7. Comparison between CIC and ESP control depending on uncertainty.

feasible stiffness values. The results suggest that the ESP control achieve higher stiffness values for lower uncertainty ratios, but the achievable stiffness diminishes as the uncertainty ratio increases.

The passivity condition of the R-ESP control can be evaluated by calculating the closed-loop function in the presence of uncertainty. The closed-loop impedance in the Laplace domain is represented as:

$$Z_{unct}^{R-ESP}(s) = \frac{1}{P_l s} + \frac{N^2(K K_q K_n^{-1} + K) P_m^{-1} + K K_q}{N^2 P_m^{-1} + K + Q(K_n - K)} \frac{1}{s}. \quad (25)$$

The Q filter can be approximated as 1 when its cut-off frequency is set to a high value. Under this assumption, the real part of the impedance in (25) is derived as follows:

$$\Re(Z_{unct}^{R-ESP}) = \frac{B_m K N^{-2} (K_n K_q K_n^{-1} + K_n - K_q)}{(B_m \omega)^2 + (N^{-2} K - J_m \omega^2)^2}. \quad (26)$$

A comparison between the closed-loop impedance between the R-ESP and that of the ESP in (23) reveals that the K term within the parentheses of the numerator in (23) has been replaced by K_n in (26). Consequently, in the case of the R-ESP, the above equation consistently yields a positive value. In conclusion, the maximum achievable stiffness with the ESP controller is limited due to stiffness uncertainty, while the R-ESP theoretically guarantees an infinite achievable stiffness, irrespective of this uncertainty.

B. Stability analysis considering filter

Due to the non-collocated nature of the load position in the SEA, it is challenging to achieve a significant increase in the feedback gain without risking system instability. This challenge becomes evident when examining the phase of the frequency response. To evaluate the phase characteristics, a transfer function from the motor input to the load position is derived as follows:

$$T_{m2q}(s) = \frac{q}{\tau_m} = \frac{N^{-1} K}{P_m^{-1} P_l^{-1} + K P_m^{-1} + K N^{-2} P_l^{-1}}. \quad (27)$$

The denominator of the function is organized in a 4-th order, causing a phase drop of -360° . The gain margin is constrained by this phase drop. The ESP control improves the phase characteristics of the load position feedback. The utilization of the ESP control in the transfer function ($T_{ESP} T_{m2q}$) results in a shift of the minimum phase from -360° to

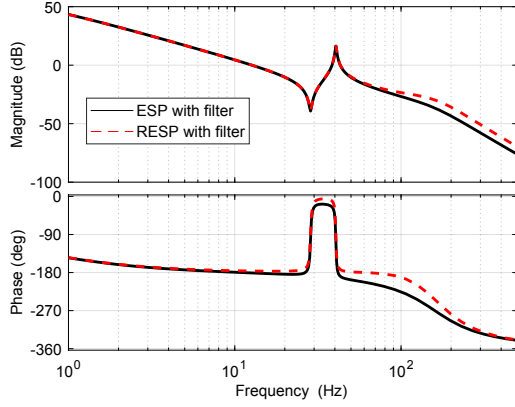


Fig. 8. Frequency response of ESP and R-ESP considering filter.

-180° , effectively enhancing system stability. Nonetheless, the introduction of a second-order differentiating filter can potentially compromise stability. Hence, it is crucial to conduct a thorough stability analysis of both the ESP and the R-ESP control. The subsequent analysis emphasizes the benefits of the R-ESP in alleviating the stability concern caused by the filter.

The ESP and DOB filters applied to the R-ESP control are defined as follows:

$$Q_{ESP} = \frac{\omega^2}{s^2 + 2\zeta_{ESP}\omega s + \omega^2}, Q = \frac{\omega^2}{s^2 + 2\zeta_{DOB}\omega s + \omega^2}. \quad (28)$$

where ω represents a cutoff frequency of ESP and DOB filters, and ζ are a damping ratio of the filters.

A transfer function for the load position ($T_{\beta 2q}$) in relation to the new input by the ESP (β) is derived as follows:

$$T_{\beta 2q}(s) = \frac{q}{\beta} = \frac{Q_{ESP}(P_m^{-1} + N^{-2}K)}{P_m^{-1}P_l^{-1} + KP_m^{-1} + KN^{-2}P_l^{-1}}. \quad (29)$$

The Q filter of the ESP (Q_{ESP}) is included to the numerator and directly disrupts the phase. A transfer function for the R-ESP is also derived as follows:

$$T_{\beta 2q}(s) = \frac{q}{\beta} = \frac{[Q + (1-Q)Q_{ESP}](P_m^{-1} + N^{-2}K)}{P_m^{-1}P_l^{-1} + KP_m^{-1} + KN^{-2}P_l^{-1}}. \quad (30)$$

In Equation (30), the numerator is made up of two components: the dynamics term and a composite of filters Q and Q_{ESP} . The composition of the filter in the numerator distinguishes the frequency response of the R-ESP from that of the ESP, as shown in Fig. 8. This result shows that the R-ESP control provide a greater phase margin than ESP control. It should be noted that the gain margin is the maximum achievable stiffness that is stably rendered, as the controllers feeds back the equation ($T_{\beta 2q}$) by multiplying the desired stiffness. Accordingly, we can conclude that the R-ESP reliably render greater impedance stiffness when considering the filter.

Analytically deriving optimal filter parameters is difficult due to the complexity of a transfer function; however, numerically determining the maximum achievable stiffness can effectively investigate the impact of these filter parameters. Figure 9 illustrates the maximum achievable stiffness depending on filter parameters (ζ , ω) when using the R-ESP controller. The pole of the impedance transfer function is

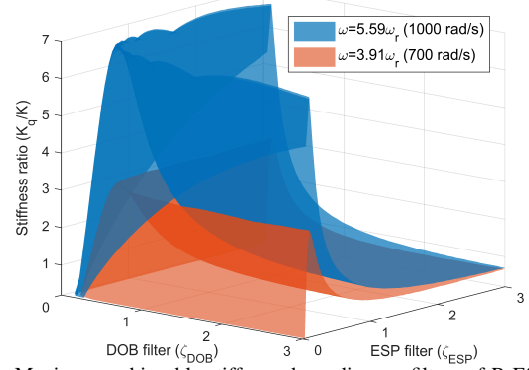


Fig. 9. Maximum achievable stiffness depending on filters of R-ESP.

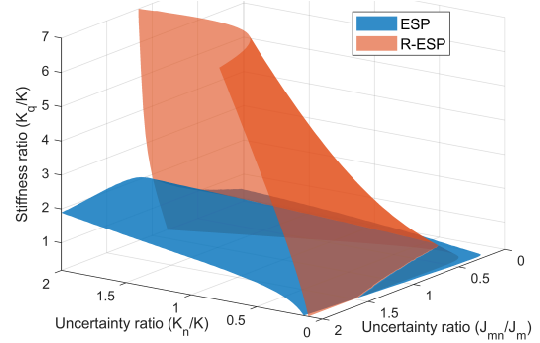


Fig. 10. Maximum achievable stiffness depending on stiffness and motor inertia uncertainty.

utilized for numerical calculations to determine the maximum achievable stiffness. A red area represents the condition where the frequency (ω) is set to 700 rad/s, while a blue area indicates a frequency of 1000 rad/s, which are 3.91 times and 5.59 times the resonance frequency (ω_r) respectively. These colored surfaces indicate the maximum achievable stiffness, with all areas below these surfaces representing achievable stiffness. The results show that as the filter frequency (ω) rises, there is a corresponding increase in the maximum achievable stiffness across all values. Optimal damping ratio values (ζ_{ESP} , ζ_{DOB}) can be obtained based on the determined frequency. It is noteworthy that the maximum stiffness is achieved when both damping ratios for the DOB and ESP filters are set to less than 1, not at the critical damping condition. Consequently, the damping ratio can be optimized: the optimal values for damping ratio are 0.38 for both frequencies of 700 rad/s and 1000 rad/s.

Figure 10 displays the maximum achievable stiffness depending on uncertainties in stiffness and motor inertia. The filter frequency is set at 1000 rad/s and damping ratios are set to the optimal values. The results demonstrate that increasing stiffness uncertainty leads to higher maximum achievable stiffness for both ESP and R-ESP control. Figures 7 and 10 show contrasting results of stiffness uncertainty on maximum stiffness due to different analysis methods: passivity in Fig. 7 and stability with filters in Fig. 10. It is necessary to consider and meet the conditions in both analyses. For the motor, the maximum achievable stiffness decreases as the motor inertia uncertainty decreases. Thus, it is recommended to set the nominal values equal to or greater than the system value for

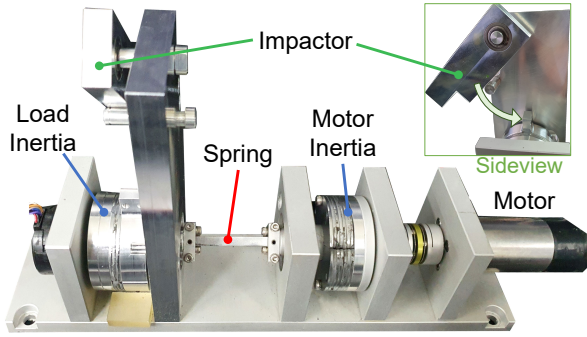


Fig. 11. Experimental setup of two-mass system.

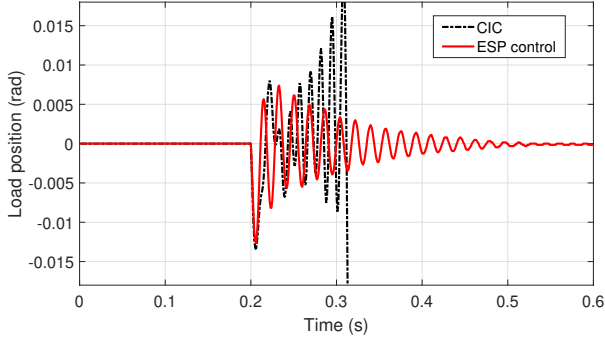


Fig. 12. Impulse responses of cascade impedance control and ESP control ($K_q = 1.2K$).

safe implementation. Importantly, the R-ESP control exhibits a superior maximum achievable stiffness in a large area than the ESP control.

V. EXPERIMENT RESULTS

This section presents four experiments. The first compares the stiffness rendering of CIC and ESP control, while the subsequent two demonstrate the effectiveness of R-ESP control in mitigating motor-side disturbances and model uncertainty. The final experiment verifies the repeatability of controllers under various stiffness settings. A two-mass system serves as experimental setup, as shown in Fig. 11, which represents the fundamental structure of a SEA; a motor and a load interconnected by a spring. To determine the spring deflection, the deflection between the motor and load is measured by encoder readings. The damping coefficients of the motor (D_η) and load (D_q) are established as $4.68e-03$ Nm·s/rad and $3.12e-03$ Nm·s/rad, respectively. The other parameters are set to the same values as in the simulation.

In our first experiment, we employed a load impactor to generate reproducible impacts of specific magnitudes. This setup allows for a comparative analysis of the impulse response between CIC and ESP controls. Figure 12 presents the experimental results in terms of the measured load position in response to an impact. Both CIC and ESP controls are parameterized so that the desired stiffness (K_q) exceeds the spring stiffness (K). Our experimental results, as summarized in Fig. 12, clearly demonstrate that, when exposed to identical disturbances, the CIC control system exhibits instability, while the ESP controller consistently demonstrates stable performance.

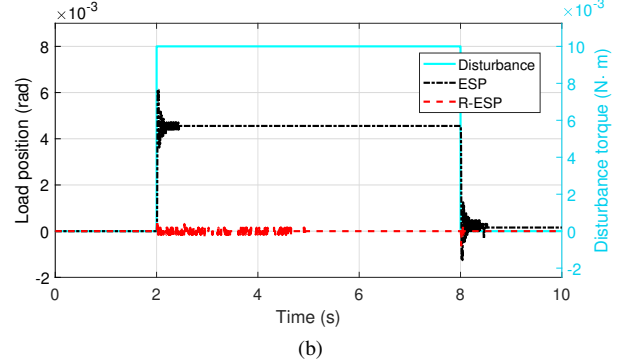
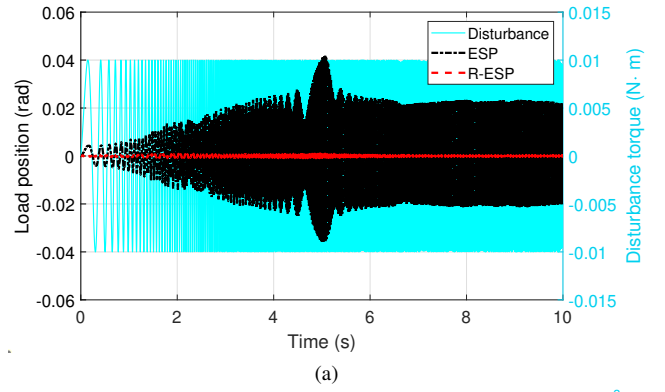


Fig. 13. Disturbance rejection performance in the ESP and Robust ESP when (a) a chirp and (b) a step disturbance exist ($K_q = K$).

The second experiment compares the performance of ESP and R-ESP control to reject motor-side disturbances in two different scenarios. In the first scenario, we applied impedance and intentionally applied a chirp wave disturbance ranging from 0 to 100Hz into the motor input, as depicted in Fig. 13(a). In the second scenario, we again applied impedance, but applied a step-wise disturbance after two seconds, lasting for a duration of 6 seconds, as indicated in Fig. 13(b). The results unmistakably demonstrate that the R-ESP control exhibits superior disturbance rejection capabilities for both disturbance cases. These outcomes underscore that we succeeded with our objective of improving the motor-side disturbance rejection behavior of ESP control.

The third experiment compares the impulse responses of R-ESP and ESP control systems in the presence of uncertainties related to motor inertia and joint stiffness parameters. Both ESP and R-ESP control are set to render an impedance during the experiment, and an impulse-like external force was applied to the load-side using the impactor at 0.2 seconds. Under significant stiffness uncertainty ($K_n = 2K$), the ESP performance deteriorated notably, as evident in Figure 14(a), whereas the R-ESP exhibits stable behavior. Under motor inertia uncertainty ($J_{mn} = 1.3J_m$), only the R-ESP controller remained stable, as shown in Fig. 14(b). These results align with the analysis in Sec. IV and confirm that we have achieved our second objective, which was to increase the robustness of ESP designs with respect to model parameter uncertainty.

To ensure repeatability, experiments under four different stiffness settings were repeated 10 times for each controller. The vibration magnitude was captured at 0.3 seconds after

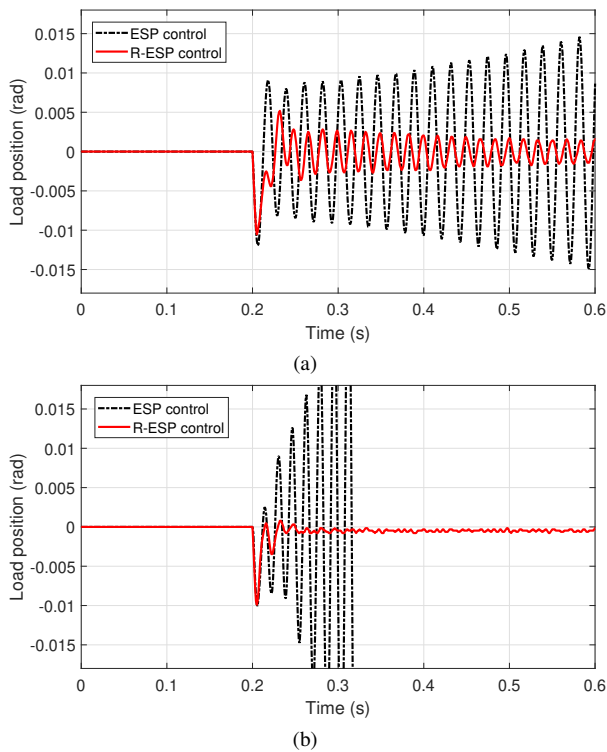


Fig. 14. Impulse responses of ESP and R-ESP control (a) with stiffness uncertainty ($K_n = 2K, K_q = 2K$) and (b) with motor inertia uncertainty ($J_{mn} = 1.3J_m, K_q = 1.5K$).

TABLE I
MEAN AND STANDARD DEVIATION VALUES FROM TEN TRIALS UNDER DIFFERENT NOMINAL STIFFNESS CONDITIONS.

		$K_n=0.8K$	$1K$	$1.5K$	$2K$
ESP	Mean	0.2 (limit)	0.2 (limit)	0.0828	0.0145
	STD	0	0	0.0018	0.0023
R-ESP	Mean	3.691e-04	2.513e-04	2.356e-04	2.505e-03
	STD	4.287e-04	9.397e-04	1.385e-04	3.130e-04

observing the impulses. The mean and standard deviation values of these measurements were then calculated as in table I. To protect the test bed, a load position limit of 0.2 rad was implemented. In the ESP control, all conditions exhibit instability. The R-ESP demonstrates consistent stable behavior across multiple trials, as indicated by the small mean and standard deviation values.

VI. CONCLUSIONS

This paper has proposed the robust control approach for series elastic actuators. The characteristics of the existing Elastic Structure Preserving algorithm were analyzed in the frequency domain and its impedance rendering was compared with the cascade impedance control. Furthermore, the robust ESP control was developed to provide the function of disturbance rejection in the basic ESP control. The robustness of the proposed controller was confirmed through experiments, demonstrating its superior ability to handle uncertainty and achieve higher impedance rendering.

REFERENCES

[1] G. Pratt and M. Williamson, "Series elastic actuators," in *IEEE/RSJ IEEE/RSJ Int. Conf. Intell. Robots Syst.*, vol. 1, pp. 399–406 vol.1, 1995.

[2] J. Pratt, B. Krupp, and C. Morse, "Series elastic actuators for high fidelity force control," *Industrial Robot: Int. J.*, vol. 29, no. 3, pp. 234–241, 2002.

[3] S. Oh and K. Kong, "High-precision robust force control of a series elastic actuator," *IEEE/ASME Trans. Mechatron.*, vol. 22, no. 1, pp. 71–80, 2017.

[4] N. Paine, J. S. Mehling, J. Holley, N. A. Radford, G. Johnson, C.-L. Fok, and L. Sentis, "Actuator control for the nasa-jsc valkyrie humanoid robot: A decoupled dynamics approach for torque control of series elastic robots," *Journal of Field Robotics*, vol. 32, no. 3, pp. 378–396, 2015.

[5] J. Lee, A. Ajoudani, E. M. Hoffman, A. Rocchi, A. Settini, M. Ferrati, A. Bicchi, N. G. Tsagarakis, and D. G. Caldwell, "Upper-body impedance control with variable stiffness for a door opening task," in *14th IEEE-RAS Int. Conf. Humanoid Robots*, pp. 713–719, 2014.

[6] S. Wang, L. Wang, C. Meijneke, E. Van Asseldonk, T. Hoellinger, G. Cheron, Y. Ivanenko, V. La Scaleia, F. Sylos-Labini, M. Molinari, et al., "Design and control of the mindwalker exoskeleton," *IEEE Trans. Neural Syst. Rehabil. Eng.*, vol. 23, no. 2, pp. 277–286, 2015.

[7] H. K. Kwa, J. H. Noorden, M. Missel, T. Craig, J. E. Pratt, and P. D. Neuhus, "Development of the ihm mobility assist exoskeleton," in *IEEE Int. Conf. Robot. Autom.*, pp. 2556–2562, 2009.

[8] G. Metta, G. Sandini, D. Vernon, L. Natale, and F. Nori, "The icub humanoid robot: an open platform for research in embodied cognition," in *8th Workshop Perform. Metrics Intell. Syst.*, pp. 50–56, 2008.

[9] H. Lee, S. Kwak, and S. Oh, "Force control of series elastic actuators-driven parallel robot," in *Proc. IEEE Int. Conf. Robot. Autom.*, pp. 1–5, May 2018.

[10] H. Vallery, J. Veneman, E. Van Asseldonk, R. Ekkelenkamp, M. Buss, and H. Van Der Kooij, "Compliant actuation of rehabilitation robots," *IEEE Robotics & Automation Magazine*, vol. 15, no. 3, 2008.

[11] D. P. Losey and M. K. O'Malley, "Effects of discretization on the k-width of series elastic actuators," in *IEEE Int. Conf. Robot. Autom.*, pp. 421–426, 2017.

[12] N. L. Tagliamonte and D. Accoto, "Passivity constraints for the impedance control of series elastic actuators," *J. Syst. Control Eng.*, vol. 228, no. 3, pp. 138–153, 2014.

[13] A. Calanca, R. Muradore, and P. Fiorini, "Impedance control of series elastic actuators: Passivity and acceleration-based control," *Mechatronics*, vol. 47, pp. 37–48, 2017.

[14] J. E. Colgate, *The control of dynamically interacting systems*. PhD thesis, Massachusetts Institute of Technology, 1988.

[15] F. Sergi and M. K. O'Malley, "On the stability and accuracy of high stiffness rendering in non-backdrivable actuators through series elasticity," *Mechatronics*, vol. 26, pp. 64–75, 2015.

[16] A. Asignacion, K. Haninger, S. Oh, and H. Lee, "High-stiffness control of series elastic actuators using a noise reduction disturbance observer," *IEEE Trans. Ind. Electron.*, vol. 69, no. 8, pp. 8212–8219, 2021.

[17] D. P. Losey, A. Erwin, C. G. McDonald, F. Sergi, and M. K. O'Malley, "A time-domain approach to control of series elastic actuators: Adaptive torque and passivity-based impedance control," *IEEE/ASME Trans. Mechatron.*, vol. 21, no. 4, pp. 2085–2096, 2016.

[18] M. Keppler, D. Lakatos, C. Ott, and A. Albu-Schaffer, "Elastic structure preserving (esp) control for compliantly actuated robots," in *IEEE/RSJ Int. Conf. Intell. Robots Syst.*, pp. 5861–5868, IEEE, 2018.

[19] M. Keppler, C. Raschel, D. Wandering, A. Stemmer, and C. Ott, "Robust stabilization of elastic joint robots by esp and pid control: Theory and experiments," *IEEE Robotics and Automation Letters*, vol. 7, no. 3, pp. 8283–8290, 2022.

[20] M. Keppler, C. Ott, and A. Albu-Schaffer, "From underactuation to quasi-full actuation: Aiming at a unifying control framework for articulated soft robots," *Int. J. Robust Nonlinear Control*, vol. 32, no. 9, p. 5453–5484, 2022.

[21] H. Lee, J.-H. Ryu, J. Lee, and S. Oh, "Passivity controller based on load-side damping assignment for high stiffness controlled series elastic actuators," *IEEE Trans. Ind. Electron.*, vol. 68, no. 1, pp. 871–881, 2021.

[22] M. Keppler, D. Lakatos, C. Ott, and A. Albu-Schaffer, "Elastic structure preserving (esp) control for compliantly actuated robots," *IEEE Trans. Robotics*, vol. 34, pp. 317–335, April 2018.

[23] K. Ohnishi, M. Shibata, and T. Murakami, "Motion control for advanced mechatronics," *IEEE/ASME Trans. Mechatron.*, vol. 1, no. 1, pp. 56–67, 1996.

[24] C. Lee, D. Cheon, and S. Oh, "High fidelity impedance control of series elastic actuator for physical human-machine interaction," in *45th Annu. Conf. IEEE Ind. Electron. Soc.*, vol. 1, pp. 3621–3626, IEEE, 2019.